LLNL-JRNL-738072

LAWRENCE LIVERMORE NATIONAL LABORATORY

The influence of hydraulic fracturing in carbon storage performance

P. Fu, R. R. Settgast, Y. Hao, J. P. Morris, F. J. Ryerson

September 6, 2017

Journal of Geophysical Research

The influence of hydraulic fracturing on carbon storage performance

Pengcheng Fu[1], Randolph R. Settgast, Yue Hao, Joseph P. Morris, and Frederick J. Ryerson

[1]Atmospheric, Earth, and Energy Division, Lawrence Livermore National Laboratory, USA.

Corresponding author: Pengcheng Fu (fu4@llnl.gov)

Key Points:

- The enabling condition, processes, and mechanisms of caprock hydraulic fracturing during CO_2 injection are investigated.
- Vertically-contained hydraulic fractures provide an effective means to access reservoir volume far from the injection well.
- Geomechanically contained caprock fracture could improve storage performance in lower-perm. reservoirs while maintaining GCS integrity.

Fu, P., Settgast, R. R., Hao, Y., Morris, J. P., & Ryerson, F. J. (2017). The influence of hydraulic fracturing on carbon storage performance. Journal of Geophysical Research: Solid Earth, 122. DOI: 10.1002/2017JB014942

Abstract

Conventional principles of the design and operation of geologic carbon storage (GCS) require injecting CO_2 below the caprock fracturing pressure to ensure the integrity of the storage complex. In non-ideal storage reservoirs with relatively low permeability, modest injection rates can lead to pressure buildup and hydraulic fracturing of the reservoir and caprock. While the GCS community has generally viewed hydraulic fractures as a key risk to storage integrity, a carefully-designed stimulation treatment under appropriate geologic conditions could provide improved injectivity while maintaining overall seal integrity. A vertically-contained hydraulic fracture, either in the reservoir rock or extending a limited height into the caprock, provides an effective means to access reservoir volume far from the injection well. Employing a fully-coupled numerical model of hydraulic fracturing, solid deformation, and matrix fluid flow, we study the enabling conditions, processes, and mechanisms of hydraulic fracturing during CO_2 injection. A hydraulic fracture's pressure-limiting behavior dictates that the near-well fluid pressure is only slightly higher than the fracturing pressure of the rock and is insensitive to injection rate and mechanical properties of the formation. Although a fracture contained solely within the reservoir rock, with no caprock penetration, would be an ideal scenario, poroelastic principles dictate that sustaining such a fracture could lead to continuously increasing pressure until the caprock is fractured. We also investigate the propagation behavior and injection pressure responses of a hydraulic fracture propagating in a caprock subjected to heterogeneous *in situ* stress. The results have important implications for the use of hydraulic fracturing as a tool for managing storage performance.

1 Introduction

Geologic carbon sequestration (GCS) requires injecting large volumes of carbon dioxide (CO_2) in deep geologic formations to prevent its release to the atmosphere [Orr, 2009; Haszeldine, 2009]. The deployment of GCS at a massive scale (billions of tonnes of CO_2 annually) is considered a critical means of greenhouse gas control over the next few decades [Pacala & Socolow, 2004; IEA 2010]. CO_2 storage targets are typically saline aquifers or depleted oil/gas reservoirs overlain by low permeability caprocks. Deep saline aquifers are expected to have the largest storage potential [McGrail et al., 2006; Celia et al., 2015]. An essential consideration in the design and operation of a CO_2 storage complex is to secure the integrity of the caprock to prevent CO_2 leakage from the storage reservoir. It is well known that hydraulic fractures may initiate and propagate in the caprock when fluid pressure exceeds the minimum *in situ* principal stress (S_{hmin}) of the caprock [Hubbert & Willis, 1957]. To avoid compromising seal integrity, a typical strategy is to strictly limit the downhole injection pressure below the estimated fracturing pressure of the caprock. However, high injection pressure could be necessary or desirable given practical and economic considerations. There is thus an inherent tension between maximizing injection efficiency and minimizing leakage risk. This is particularly true for reservoirs with relatively low permeabilities and consequently low injectivities. To date, high permeability reservoirs that provide favorable injection and storage conditions have been favored for use in CO_2 sequestration projects, such as the Sleipner and Snøhvit sites [Boait et al., 2012; Eiken et al., 2011; Verdon et al., 2013; Chiaramonte et al., 2015]. However, significant reduction in global greenhouse gas emission requires extremely large volumes of CO_2 injection [Pacala & Socolow, 2004; Ehlig-Economides & Economides, 2010; Zoback & Gorelick, 2012], and therefore saline aquifers with a wide spectrum of permeabilities, including relatively low permeabilities, will have to be considered. Existing CO_2 sequestration projects have encountered reservoir permeabilities as low as one millidarcy [Verdon et al. 2013] creating challenging storage conditions. An important case study in this context is the In Salah project [Ringrose et al. 2013]. Comprehensive analyses of monitoring data---including injection pressure, surface deformation, tracers, microseismic, and 4D seismic---suggest that one or more hydraulic fractures may have been created in the reservoir and lower caprock system during injection operations [Bissell et al. 2011, Oye et al. 2013, White et al. 2014, Bohloli et al. 2017]. An alternative hypothesis is that a pre-existing fracture zone (or fault) was re-activated [Iding & Ringrose 2010; Morris et al., 2011; Shi et al., 2012]. In either case, it is evident that the resulting conductive feature had a limited vertical extent within the lower portion of caprock and did not cause detectable leakage of CO_2 out of the storage complex.

Although conventional wisdom calls for strict prevention of caprock hydraulic fracturing, it is of great importance to understand 1) the conditions that lead to caprock hydraulic fracturing, 2) the effects of geologic characteristics and operational parameters on the propagation of caprock fractures, and 3) the role of hydraulic fractures in CO_2 storage reservoir's responses to injection and reservoir management measures. There are clearly reservoir configurations where hydraulic fracturing would be an unacceptable risk to storage integrity, and others where it could be a useful tool to maximize injection efficiency and stored volumes.

A growing hydraulic fracture is an intricate mechanical system consisting of deforming rock, flowing fluid in both the fracture and rock matrix, and a propagating discontinuity. The body of literature describing the complex nature (complex even in idealized settings) of hydraulic fractures [e.g., Perkins & Kern, 1961; Nordgren, 1972; Renshaw & Harvey, 1994; Detournay 2004; Zhang & Jefferey, 2012; Lecampion et al., 2017] testifies the challenge of studying subsurface processes involving these features. However, past research in CO_2 sequestration has largely overlooked many characteristics of hydraulic fractures and their potential effect on the CO_2 storage system.

Most work in GCS to date has treated hydraulic fractures in a simplified manner as a fixed-size, "equivalent" porous zone---essentially treating it as a vertical wing of the reservoir [e.g., Morris et al., 2011; Durcan et al., 2011; Pan et al., 2013; Rinaldi & Rutqvist, 2013]. Here, we employ a more realistic numerical model to investigate the fundamental behavior of caprock hydraulic fracturing and its impact on a reservoir's response to CO_2 injection. The model captures dynamic interactions between a propagating fracture, solid rock deformation, fluid flow along the fracture, and leak-off of fluids into the surrounding formations. Our model still contains significant simplifications, however, especially with respect to the multiphase and non-isothermal behavior of CO_2-brine systems. Nevertheless, the model provides physical insights into the hydro-mechanical behavior of a fractured storage system, and is intended to prompt a more robust analysis in the GCS community of the advantages and disadvantages of hydraulic fracturing as an engineering tool.

The modeling and analysis in this work is based on the assumption of vertical containment of the hydraulic fracture at a finite distance above the reservoir, as we intend to study the influence of such vertically contained hydraulic fractures. The mechanisms of vertical containment of hydraulic fracture are complex and a subject of active research in its own right. Generally, vertical propagation of a hydraulic fracture can be halted by geologic discontinuities and/or stress contrast between adjacent formations [Fisher&Warpinski, 2012; Warpinski et al., 1982; Warpinski&Teufel, 1987].

The structure of the paper is as follows. Sections 2 and 3 describe the numerical simulation methodology and the setup of a baseline case study. Section 4 analyzes the conditions that lead to caprock hydraulic fracturing. Section 5 presents results for a propagating caprock hydraulic fracture (using the baseline model) and its interaction with the reservoir. Section 6 analyzes the key physical controls on the hydraulic fracture/reservoir interactions to inform an analytical equation predicting the growth of the caprock hydraulic fracture. The effects of the distribution of *in situ* stress in the caprock on hydraulic fracturing propagation are studied in section 7. A summary of this work and discussions of its implications are offered in section 8.

2 Simulation methodology

A simulation of hydraulic fracturing, including interaction with a high-permeability porous reservoir, must capture a number of coupled processes: 1) solid deformation of the rock layers, 2) fluid flow in the porous media, 3) fluid flow along the fracture, and 4) the deformation and propagation of the fracture. Here, we model the rock as a linear elastic medium deforming quasi-statically. From the start, we make a significant simplification and model fluid flow in the CO_2-brine system with a quasi-single-phase model. We recognize that this approach ignores important multiphase interactions occurring as supercritical CO_2 floods a brine-saturated reservoir, such as buoyancy-driven flow [Bryant et al., 2008; Okwen et al., 2011]. Nevertheless, such processes are not necessarily important for the conditions considered in this work (i.e. low permeability, thin reservoir) and this simplified approach still provides valuable insight into the hydro-mechanical behavior of such a system. We note that tools to model the complete physics of a fracturing CO_2 storage system do not yet exist and are the subject of current development.

Here, we briefly review the governing equations and discretization strategy. The model consists of a porous domain, *m*, penetrated by a discrete surface, *f*, representing a growing fracture (Figure 1). The primary unknowns are the solid displacement $\boldsymbol{u}$, fluid pressure in the porous matrix p_m, and fluid pressure in the fracture p_f. The fracture aperture w is related to the displacement field as

$$w = [\![\boldsymbol{u}]\!] \cdot \boldsymbol{n} \qquad (1)$$

where $[\![\boldsymbol{u}]\!] = (\boldsymbol{u}^+ - \boldsymbol{u}^-)$ is the jump in the displacement field across the fracture surface, and $\boldsymbol{n}$ is the normal vector to the fracture surface. The unknown fields must satisfy

$$\nabla \cdot \boldsymbol{\sigma} + \rho \boldsymbol{g} = \boldsymbol{0} \qquad \text{(2, momentum balance in the matrix)}$$

$$\frac{\mathrm{d}}{\mathrm{d}t}(\rho_m \phi) + \nabla \cdot (\rho_m \boldsymbol{w}_m) = 0 \qquad \text{(3, mass balance in the matrix)}$$

$$\frac{\mathrm{d}}{\mathrm{d}t}\left(\rho_f w\right) + \nabla_f \cdot (\rho_f \boldsymbol{w}_f) = q_i - q_{fm} \qquad \text{(4, mass balance in the fracture)}$$

$$\boldsymbol{\sigma} \cdot \boldsymbol{n} = -p_f \cdot \boldsymbol{n} \qquad \text{(5, traction balance across the fracture)}$$

$$[\![\rho_m \boldsymbol{w}_m]\!] \cdot \boldsymbol{n} = q_{fm} \qquad \text{(6, flux balance across the fracture)}$$

Here, $\boldsymbol{\sigma}$ is the total stress, ρ is the mixture density, ρ_m is the matrix fluid density, ϕ is the matrix porosity, $\boldsymbol{w}_m$ is the superficial (Darcy) flux in the matrix, ρ_f is the fracture fluid density, $\boldsymbol{w}_f$ is the fluid flux in the fracture, q_i is a fluid source due to injection, q_{fm} is a fluid sink due to leak-off from fracture to matrix, and ∇_f is the fracture surface gradient operator. The primary unknowns and secondary variables are related through the additional relationships, including linear elasticity for solid deformation, the principle of effective stress, Darcy's law for flow in matrix, and the "cubic-law" for fracture flow. Note that the sink term q_{fm} in equation (4) represents fluid mass vanishing from the fracture flow system but entering the porous medium flow through equation (6). As the fracture flow equations and porous medium floe equations are solved together, linked through this fluid exchange term q_{fm}, system-wide fluid mass conservation is satisfied.

We use a rock compressibility term in the porous medium flow model [Zimmerman, 2002] as a simplified version of poroelasticity, in which the volumetric strain's impact on the solid porosity is not directly calculated from the displacement field, but is instead estimated using the pressure change. It is an appropriate treatment in this context because the total stress in the system does not change significantly. Therefore, the change of the mean effective stress happens to be the pore pressure change. This leads to a one-way coupling in which the matrix mass balance equation only depends on pressures, while the momentum balance depends on both displacements and pressures. The generation of excess pore pressure when rock experiences fast compression is not handled by the model. However, this phenomenon is not particularly important for the present application because such excess pore pressure in reservoir rock dissipates faster than the loading duration representative of GSC while it is sufficient to treat the loading on the largely impermeable caprock to be "undrained". The model is supplemented with appropriate initial and boundary conditions. The simulations assume isothermal conditions, although we note that heat transport could play a significant role under certain conditions [Han et al., 2010].

The present study uses GEOS, a fully coupled hydraulic fracturing simulator to discretize and solve the model equations above [Settgast et al., 2016; Fu et al., 2013]. We use the Virtual crack closure technique (VCCT) [Krueger 2004], in a modified formulation that handles confining stress [Settgast et al., 2016], to calculate energy release rate G at fracture tips. When G is greater than the critical value G_c, mostly as a result of sufficiently high fluid pressure in the fracture, the fracture extends from the tip. New fracture area is generated by duplicate the "face element" connecting two adjacent solid elements in the original continuum body. New face flow elements are thereby added to the fracture flow system, and fluid pressure from the flow element is applied to on the exposed surfaces of the solid mesh as traction boundary conditions. Momentum balance is satisfied at each time step on the current updated mesh topology whereas fluid mass conservation is satisfied across the fracture flow and porous medium flow systems. Considering the relatively long time-scales involved in the fracturing process, we adopt an implicit time-integration strategy.

As mentioned earlier, a quasi-single-phase flow model is used for simplicity. The fracture contains a surrogate fluid with properties (density, viscosity, and compressibility) representing those of CO_2 at typical reservoir conditions. In the matrix, fluid properties representing brine are adopted. Obviously, this is a substantial simplification of the multiphase behavior of a CO_2 flood. Nevertheless, the model still captures the basic interaction between a the caprock hydraulic fracture and the reservoir.

Due to the inherent complexities of this problem despite the simplified treatment of poroelasticity and multi-phase flow, the simulations are computationally expensive. The models included in the current paper range from 900,000 to 1.7 million solid elements and cost 1,000 to 7,000 core-hours to complete.

3 Model setup

The configuration of the baseline model is shown in Figure 1. The injection reservoir is 24 m thick with its top surface located at 2,000 m depth. We establish a coordinate system with the x-axis parallel to the maximum *in situ* horizontal principal stress (S_{Hmax}) direction, y-axis parallel to the minimum horizontal principal stress (S_{hmin}) direction, z-axis pointing upwards, and the origin at ground surface above the injection point (i.e. the injection point is at x=0, y=0, z=-2012 m). For simplicity, we assume the vertical gradient of S_{hmin} is the same as the hydrostatic gradient corresponding to supercritical CO_2 density in the vertical fracture. As the two gradients then cancel each other, we use a uniform S_{hmin} of 30 MPa within the fracturable portion of the caprock formation and omit gravitational terms in flow simulation. The other two *in situ* principal stress components do not play a significant role in the analysis as long as the vertical stress is greater than S_{hmin}. In the model, we place two fracturing barriers, 120 m above the reservoir top surface and at the lower boundary of the reservoir, respectively. S_{hmin} abruptly increases by 5 MPa across the barriers. Therefore, the vertical extent of the hydraulic fracture is limited within z = -2024 m to -1880 m. The hydraulic fracture, once initiated, is expected to propagate within the x-z plane (perpendicular to the S_{hmin} direction). Considering the symmetry of the problem, we only need a half model extending from 0 to 2000 m in the x-direction, from -2000 m to 2000 m in the y-direction, and from -2400 to -1400 m in the z-direction. The model boundaries are assumed impermeable to reflect the notion that a reservoir always has bounded extents (Ehlig-Economides and Economides, 2010). The mesh resolution is relatively high (6 m to 10 m) near the expected fracture trajectory, whereas element sizes progressively increase in the far field. The model contains approximately 900,000 solid elements while several hundred face elements are generated adaptively to represent the evolving fracture face.

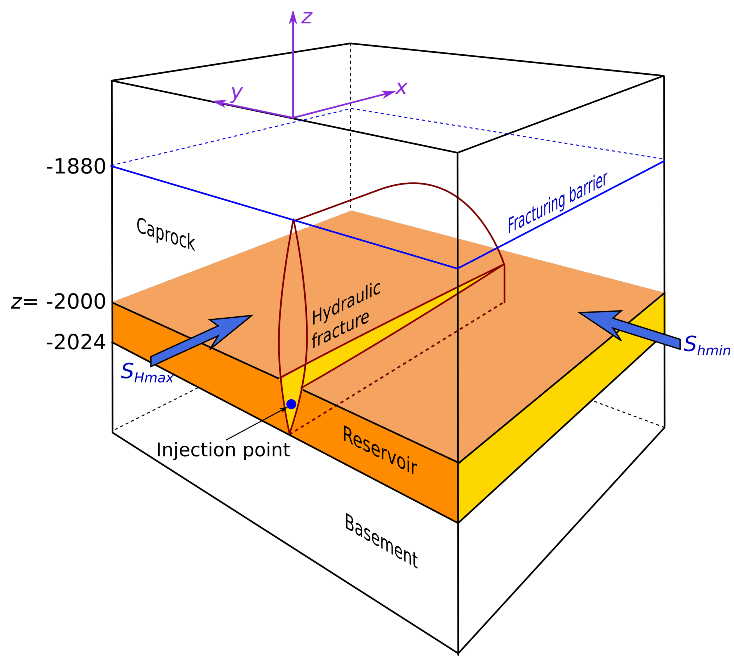

Figure 1 Configuration of the baseline model qualitatively showing the geometrical relationships between the storage reservoir, the caprock, the basement, a potential hydraulic fracture, and the orientations of the *in situ* stress. Only a half of the model (x>0) is shown due to symmetry.

Parameters used in the simulations are summarized in Table 1. All rock layers, at least in the region that is affected by the injection, are assumed to have the same mechanical properties to simplify the analysis of the baseline case. Properties of the surrogate fluid are based on the equation of state in Span and Wagner [1996] for the expected condition (supercritical state at 62°C between 20 MPa and 30 MPa) in the reservoir and in the hydraulic fracture. The simulator allows different fluid properties in the fracture flow equations and matrix flow formulation. We use a higher viscosity in the latter as the main role of pressure gradient in the reservoir is to displace brine, which is more viscous than supercritical CO_2. Table 2 is a list of the analytical and numerical models employed in this work.

Table 1 Parameters for the baseline simulation.

Property	Value
Rock Young's modulus, all formations, E	10 GPa
Poisson's ratio, all formations, v	0.25
Critical energy release rate, all formations, G_C	94 J/m^2
Porosity, reservoir, ϕ_r	0.15
Porosity, caprock and basement, ϕ_c	0.05
Permeability, reservoir, k_r	15 mD
Permeability, caprock and basement, k_c	0.01 μD
Temperature, all formations, T	62 °C
Viscosity, surrogate fluid in fracture flow, μ_f	0.1 cP
Viscosity, surrogate fluid, in porous medium flow, μ_r	0.5 cP

Total compressibility, c_t	1.25×10^{-8} Pa
Fluid density ρ_f	700 kg/m^3
Initial reservoir pore pressure, P_{ri}	20 MPa
Injection rate, q_i	0.024 m^3/s
Reservoir thickness, H_r	24 m

Table 2 A list of quantitative analyses and numerical simulations employed

Model	Section	Type	Representation of poroelasticity	Relation to baseline model
I	4	Axisymmetric, analytical	Through pore compressibility	Calculate pre-fracture pressure development based on porous medium flow theory
II	4	2D numerical	Through pore compressibility and effective stress	Poroelastic analysis of reservoir fracture re-closure
III	5	3D numerical	Through pore compressibility and fracture closure in reservoir due to poroelasticity, based on findings from Model II	Baseline model
IV	6			Greater fracture height
V	6			Shorter fracture height
VI	7			Heterogeneous *in situ* stress

4 Processes leading to caprock fracturing

A necessary condition for hydraulic fracturing in caprock is that fluid pressure exceeds S_{hmin} in the caprock in response to the reservoir condition and injection rate. For the flow of a single-phase, slightly compressible fluid from a vertical well (represented as a line source) into in infinite reservoir, a solution is given by Zimmerman [2002] in terms of dimensionless time and dimensionless overpressure as

$$\bar{t} = \frac{k_r t}{\phi_r \mu_r c_f R^2} \quad (7)$$

and

$$\bar{P}_{over} = \frac{2\pi k_r H_r (P - P_{ri})}{\mu_r q_i} \quad (8)$$

where P is the pore fluid pressure at distance R from the line source at time t after the injection has commenced. These two dimensionless quantities are connected by

$$\bar{P}_{over} = -\frac{1}{2} E_i\left(-\frac{1}{4\bar{t}}\right) \quad (9)$$

where E_i(x) is the so-called exponential integral. By assuming an injection rate of 24 liters per second or 530,000 tonnes per year and using the parameters provided in Table 1, we calculate (Model I in Table 2) the injection time required to attain various levels of overpressure at R = 24 m (choosing the formation thickness as a characteristic length scale) from the injection line source as a function of reservoir rock permeability, as plotted in Figure 2. For a reservoir with sufficiently high permeability (e.g., k_r>100 mD), the injection pressure will not reach the fracturing pressure within the time span meaningful for CO_2

injection. The results also show that lower permeability results in longer time to reach a given overpressure when the reservoir permeability is below 1 mD. This is because, although lower permeability causes higher injection pressure at the wellbore, it takes a longer time for the overpressure to propagate to the reference point at R = 24 m due to the lower hydraulic diffusivity. For the baseline model considered, the fracturing pressure of the caprock corresponds to an overpressure of 10 MPa (S_{hmin}-P_{ri}). The results show that even for a reservoir with permeability up to 30 mD, the fluid pressure at a considerable distance from the well can still attain the caprock fracturing pressure in less than half a year. For the baseline reservoir permeability assumed (15 mD), the pore fluid pressure at 24 m from the well can be more than 25 MPa (P_{over} = 5 MPa) greater than the caprock fracturing pressure within 100 days of injection.

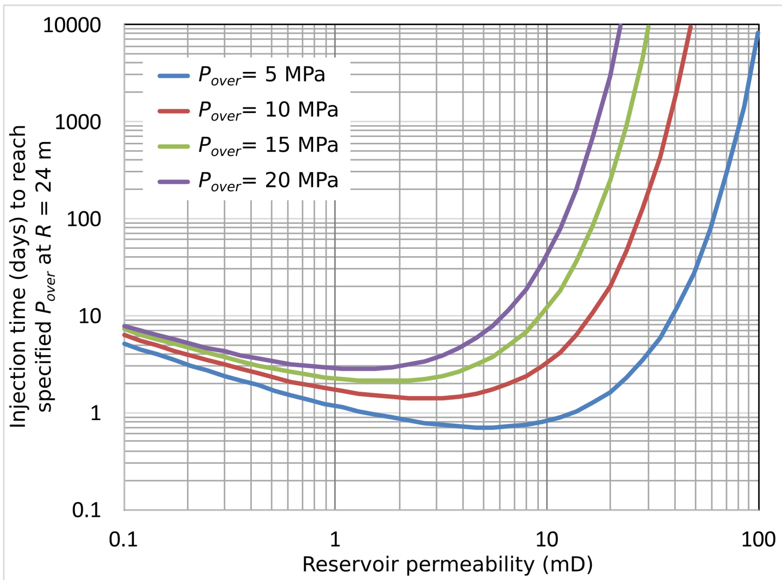

Figure 2 Under an injection rate of 24 liters per second or 530,000 tonnes per year, the required injection time to attain various levels of overpressure at R = 24 m from the injection line source as a function of reservoir rock permeability.

The above analysis assumes the condition of porous medium flow without fracturing. It is possible that hydraulic fracturing takes place in the reservoir rock formation. If the reservoir hydraulic fracturing can be sustained by a fluid pressure below S_{hmin} of the caprock, it will prevent caprock hydraulic fracturing from taking place. To understand the sustainability of a hydraulic fracture in the reservoir rock, careful consideration must be given to the poroelastic effect [Biot, 1941]. From a solid mechanics perspective, the opening of a hydraulic fracture aperture is the direct result of the compression of the rock body surrounding the fracture where higher stress (higher than the original *in situ* stress) results from the fluid pressure compressing the walls of the fracture. In the reservoir rock, the pore pressure in the compressed rock increases as the fluid flows into the rock body. Terzaghi's principle of effective stress dictates that the effective stress (which drives rock deformation) in the rock decreases in response to the pore pressure change, thereby causing relaxation of the rock compression and re-closure of the fracture aperture. It is well known that due to this poroelastic effect, pumping pressure needs to be continuously increased and significantly higher than the original S_{hmin} in the formation to sustain a hydraulic fracture in relatively permeable rocks (Detournay & Cheng, 1991; Salimzadeh et al., 2017). The poroelastic effect usually does not play a substantial role in most unconventional reservoir stimulation applications because of the low permeability of these rocks, the very reason that necessitates hydraulic fracturing stimulation. Moreover, the use of "wall-building" fluids and high-viscosity fluids reduces the distance from the fracture that is affected by pore pressure increase. However, CO_2 storage reservoirs are likely to have relatively high permeability and the fluid has low viscosity, so the poroelastic effect cannot be ignored or easily mitigated. Subsequently, we demonstrate the likely unsustainability of hydraulic fracture in the reservoir formation for the baseline parameters.

To quantitatively illustrate how the poroelastic effect affects the sustainability of a hydraulic fracture in the reservoir rock (as opposed to caprock), we simulate (Model II) the aforementioned process in the baseline model setting with some minor adjustments. We assume S_{hmin} = 30 MPa in the caprock and basement while S_{hmin} = 26 MPa in the 24 m thick reservoir. The Biot parameter is 0.8 for all rock layers. The geometry and other parameters of the system remain the same as those described in section 3. Following the analysis methodology of Detournay and Cheng [1991] we only consider a cross-section (in y-z plane) of the model shown in Figure 1. Instead of simulating the creation and relaxation of a hydraulic fracture, we assume that a fracture throughout the height of the reservoir formation already exists (Figure 4(b).) and we pressurize it with a fluid pressure of 30 MPa (approximately the pressure required to fracture the caprock or basement) at t=0. The simplifications represent the "best case scenario" for sustaining a hydraulic fracture in the reservoir rock: a fracture already exists and a higher pressure will trigger fracturing in the caprock and/or basement. Subsequently, we observe how the fracture responds to the pore pressure propagation in the reservoir.

Figure 3 (a) shows the effective stress increment perpendicular to the fracture plane (y-component) near the pressurized fracture at t=0. The blue color shows the extent of the so-called stress shadow where the rock is compressed, resulting in opening of the fracture. As the fluid pressure front propagates into the reservoir layer (Figure 3(d)), the compressive effective stress is neutralized (Figure 3(b)) and the aperture relaxes accordingly. In fact, after 4.4 hours of pressurization, the net increment of σ'_y (compared with the original state) near the fracture is tensile, meaning that the rock skeleton near the fracture has become less compressed compared with the original *in situ* state. Based on the aperture re-closure curve in Figure 3 (c), the aperture completely closes after 1.5 days of pressurization.

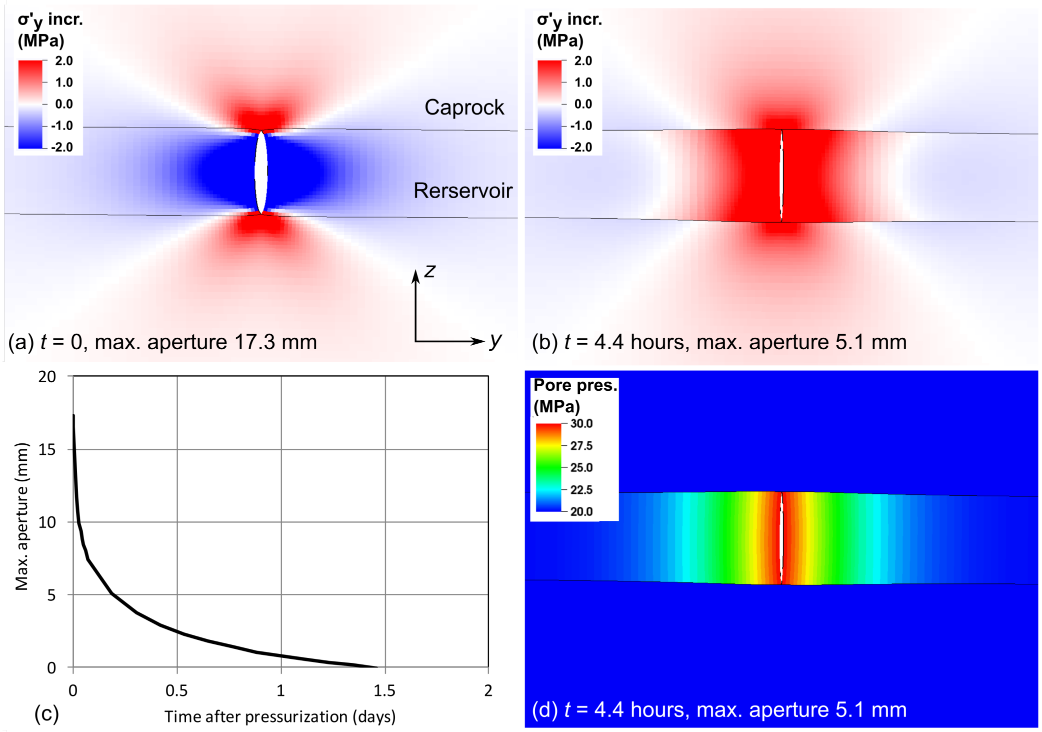

Figure 3 The aperture relaxation/reclosure of a hydraulically pressurized fracture in the reservoir formation. Only a cross-section in the y-z plane is simulated. The deformation is exaggerated by 200 times to visualize the fracture opening. (a) The increment of σ'_y (effective stress, compared with the original *in situ* stress) near the fracture at $t = 0$. Note that tensile stress is positive. (b) The σ'_y increment (still compared with the original) after 4.4 hours of pressurization. (c) The evolution of the maximum aperture with time. (d) The pore pressure distribution in the reservoir layer after 4.4 hours of pressurization. Due to the very low permeability of the caprock and basement, the Young's moduli in these layers should be seen as "undrained" modulus for the time scale considered. Poroelastic effects in these layers do not affect the results discussed here and are therefore not considered.

The above analysis assumes a constant injection pressure along a pre-existing fracture. In reality, the hydraulic fractures initiates when the injection pressure is moderately higher than S_{hmin} (26 MPa in the example), but the pressure needs to keep increasing to maintain the open fracture due to the poroelastic effect. The example shows even at a pressure of 30 MPa, the fracture can remain open only for a few days. Beyond that, the fluid pressure will soon be sufficient to fracture the caprock. Due to the caprock's low permeability, it is sufficient to consider caprock deforms in the "undrained" condition and a largely constant pressure would be sufficient to sustain the hydraulic fracture. The flow near the injection point within the reservoir will remain in the porous medium flow regime (as opposed to fracture flow) under the condition that the fluid pressure near the reservoir-caprock interface is slightly higher than S_{hmin} in the caprock.

To embody these findings in a computationally tractable yet reasonable manner in 3D, all subsequent models assume that a hydraulic fracture is not present throughout the reservoir layer (i.e. it would have been re-closed) but the caprock fracture connects to the reservoir through a 2-m high interface zone at the top of the reservoir as shown in Figure 4(c). The corresponding cross section geometries for the conceptual model in Figure 1 and Model II are shown in in Figure 4(a) and (b) for comparison. Instead of explicitly modeling the porous medium flow from the injection point to the fracture-reservoir interface, we place a "virtual source" at the interface zone above the injection point. Note that the height of the interface zone (2 m) in the model is limited by practical mesh resolutions. The selection of the interface height could have a minor effect on the simulation results through its influence on overall hydraulic impedance between the fracture and the reservoir, but is unlikely to alter how the hydraulic fracture and the reservoir communicate. The actual flow regime and mechanical response around the fluid exit from the wellbore in the reservoir formation and where fluid enters the fracture are expected to be rather complex and is beyond the scope of the current work.

Note that we only analyzed how the poroelastic effects influence the closure of the hydraulic fracture for a specific set of parameters. It is still possible that certain combination of parameters, for instance, a lower Biot's parameter and greater difference between S_{hmin} in the reservoir and the original reservoir pore pressure, can allow a sustained hydraulic fracture within the reservoir rock. This topic deserves a systematic investigation but is beyond the scope of the current work.

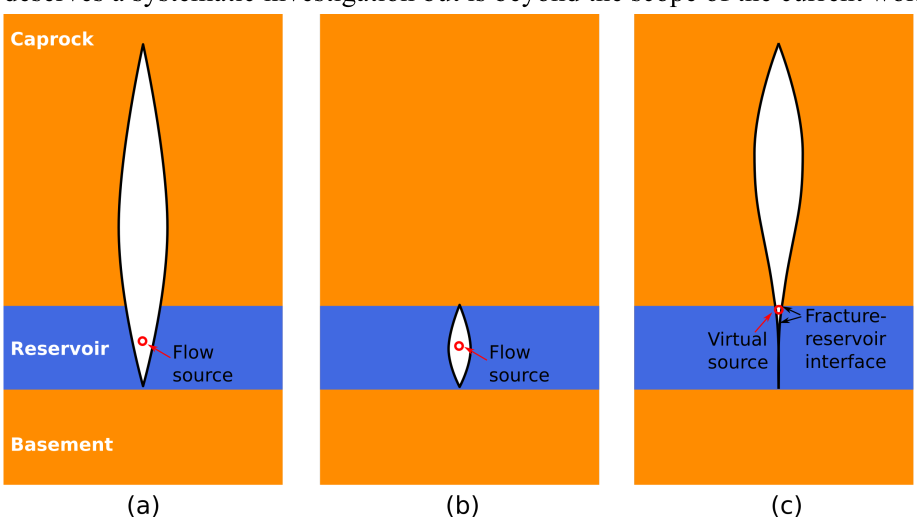

Figure 4 Various geometrical relationships between the hydraulic fracture and the storage reservoir. (a) Baseline case, fracture is open in both the reservoir and the caprock, corresponding to the imagined geometry in Figure 1. (b) The hydraulic fracuture is in the reservoir rock only, corresponding to Model II. (c) The fracture has vertically propagated into the caprock but it recloses in the reservoir rock due to poroelastic effects, corresponding to Models III to VI. The fracture and the reservoir hydraulically communicate via an open interface at the top of the reservoir rock.

5 Baseline caprock hydraulic fracturing model results

This section presents the simulation results for the baseline scenario specified in section 3 (Model III in Table 2). The aperture distribution across the growing hydraulic fracture and the reservoir pore pressure distribution after 23 days, 104 days, 208 days, and 500 days of injection are shown in Figure 5. The hydraulic fracture grows continuously with the injection, and the pressure plume in the reservoir appears to expand into the reservoir from the intersection (the 2 m high interface zone) between the hydraulic fracture and the reservoir layer. The maximum aperture and maximum fracture net pressure of the fracture modestly increase with the growth of the fracture, reaching approximately 2.4 mm and 70 kPa, respectively, after 500 days.

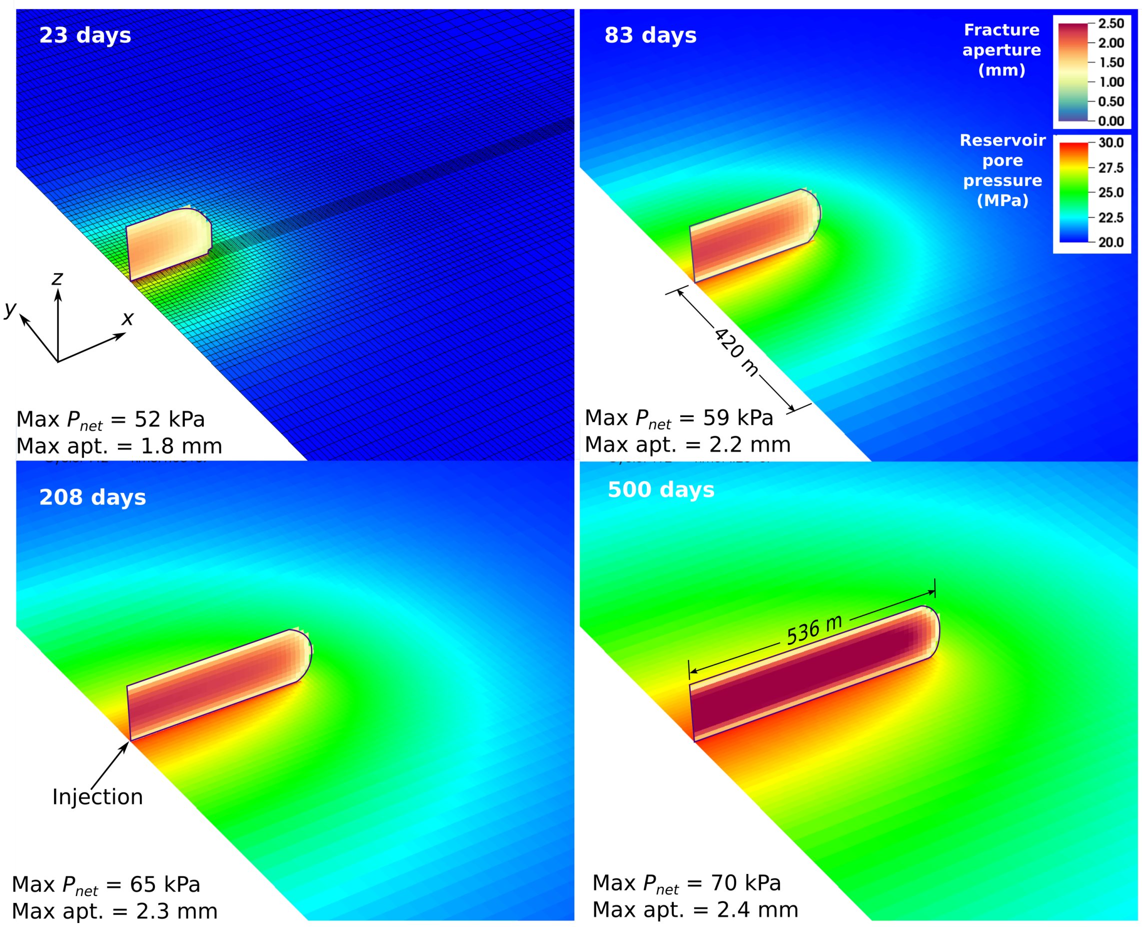

Figure 5 Aperture distribution across the growing hydraulic fracture and reservoir pore pressure at selected times into injection. Pore pressure is shown on a horizontal slice at the top of the reservoir. Element sizes can be seen on the results on day 23. At each time, the maximum fracture net pressure and the maximum aperture across the fracture are annotated. Fracture net pressure is the difference between the fluid pressure in the fracture and the original in situ normal stress on the fracture plane.

Figure 6 depicts in detail the flow fields along the hydraulic fracture at 23 days and 208 days. A few observations can be made:

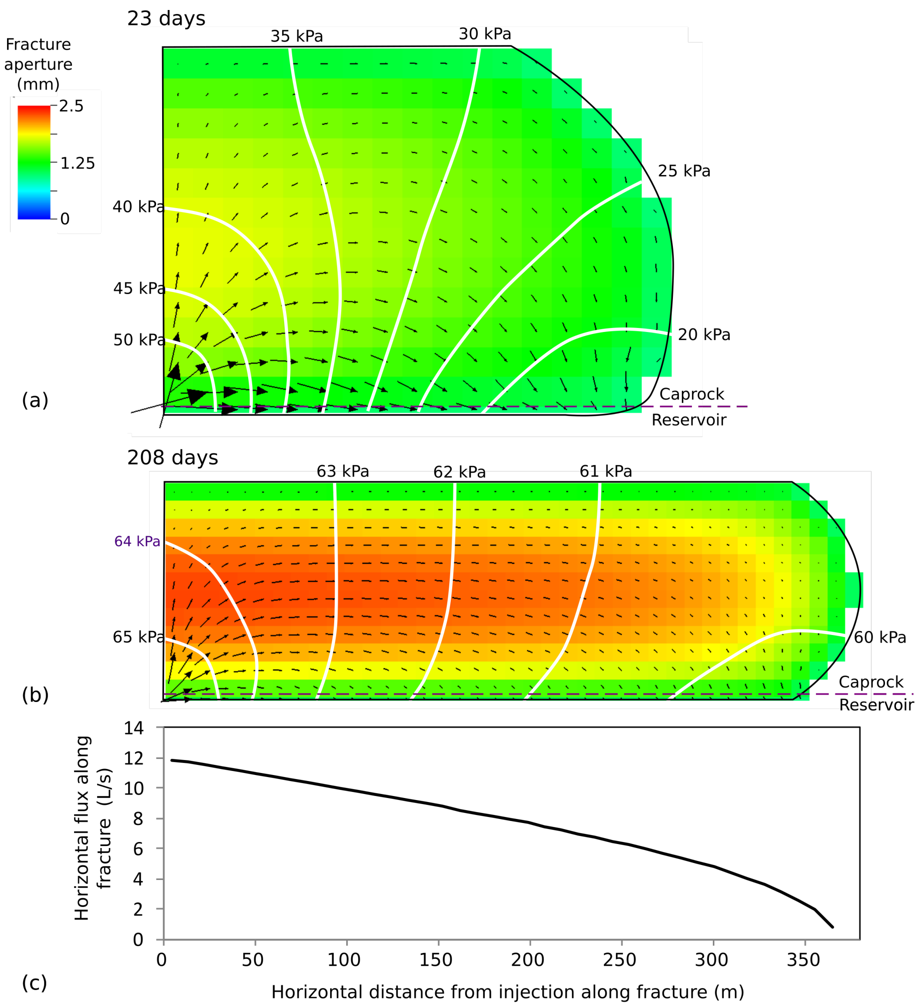

Figure 6 Detailed flow fields along the hydraulic fracture (a) 23 days and (b) 208 days into the injection. At each time, the aperture, net pressure, and flux are depicted by color, contour lines, and vectors, respectively. The fracture net pressure is defined as the difference between the fluid pressure and S_{hmin} (30 MPa). Note that the scales and aperture color maps are different between 23 days and 208 days. Also shown in (c) for 208 days is the total flux crossing the vertical cross-section of the fracture as a function of the horizontal distance from the injection point.

1) Most of the injected fluid first flows into the hydraulic fracture. As fluid flows along the fracture, it gradually leaks into the reservoir at the bottom of the fracture. The integration of the fracture flow flux across a vertical cross-section is rather close to the injection rate (12 liter/s into one wing) near the injection point. The leak-off (from fracture to reservoir) rate, on a per-fracture-length basis, increases as the distance to the injection increases. At 208 days, only about 1/3 of the fluid leaks into the reservoir in the first half of the fracture length while the other 2/3 leaks in the second half.

2) The fracture does not provide a significant storage volume for the fluid. The total storage volume of the fracture is only 95 m^3 at 208 days, less than 1/2000 of the total injected volume.

3) The net pressure along the fracture is only tens of kPa. Under the plane-strain condition, the compliance (i.e. the ratio between aperture increment and net pressure increment) of a fixed-height (H_f = 122 m in the baseline case), static fracture in is approximately $2H_f/E'$, where E' is the plane-strain modulus of elasticity. It only takes tens of kPa of net pressure to result in an aperture of several mm. According to the cubic law for fracture flow, a fracture with a 2 mm aperture has a transmissivity equivalent to 44,444 m ($0.002^3/12/15\times10^{-15}$) thick of the porous medium constituting the reservoir. Therefore, the fluid pressure only needs to slightly greater than S_{hmin}, barely opening the fracture, to attain very small hydraulic impedance along the fracture. A couple mm of aperture would provide sufficient transmissivity to allow the fluid to access the reservoir far from the injection with minimal pressure loss.

6 Propagation speed of the hydraulic fracture

The above analysis provides important insight into the role of a hydraulic fracture in the flow system. Principally, a hydraulic fracture (in reservoir or caprock or both) provides a means for the injected fluid to access the reservoir through the fracture-reservoir interface that grows with the hydraulic fracture. Across the entire fracture including the fracture-reservoir interface, the fluid pressure is approximately the same value as S_{hmin}. Due to the extreme sensitivity of a fracture's transmissivity to fracture net pressure, the fracture fluid pressure is only marginally greater than S_{hmin} for the idealized system considered so far regardless of the injection rate and rock properties. In other words, it is the difference between S_{hmin} and original reservoir pressure P_{ri} that drives the fluid into the reservoir.

Through the aforementioned mechanism, the hydraulic fracture applies a (nearly) constant-fluid pressure boundary condition along the fracture-reservoir interface area for the flow into the reservoir. It is well known that if the area over which such a constant-pressure boundary condition is applied remains constant, the flow rate into the porous medium (reservoir) decreases with time. To maintain a constant total injection rate, the interface area has to increase. Therefore, **the hydraulic fracture extends at such a rate that the associated increase of the fracture-reservoir interface area can accommodate the constant (or any) injection rate**. This is a close analogue to the PKN (Perkins-Kern-Nordgren) hydraulic fracture model in the leak-off-dominated regime [Perkins & Kern, 1961; Nordgren, 1972]. The PKN model addresses the propagation of a vertical, constant-height (H_f) hydraulic fracture, and the high-leak-off approximation of the half-length of the fracture as a function of injection time (Nordgren [1972]) is

$$L(t) = \frac{q_i t^{0.5}}{2\pi C_L H_f} \quad (10)$$

where q_i is the total injection rate (two wings combined), and C_L is the so-called Carter's leak-off coefficient of the reservoir. According to Carter [1957], the leak-off velocity at a point on the fracture into the rock matrix is

$$u_L(t) = \frac{C_L}{\sqrt{t-t_0}} \quad (11)$$

where t-t_0 is the elapsed time since the exposure of the fracture surface to the fluid. Note that the numerical models in this study use fully coupled fracture-matrix flow solution and does not use Carter's leak-off model.

The chief difference between our baseline model and the high-leak-off PKN model is that the former only allows fluid to leak through a relatively small segment of the fracture height (2 m interface out of the 122 m total height) whereas the latter assumes the entire height of the fracture constitutes the leak-off interface. Therefore, the $C_L H_f$ term in equation (16) should be replaced with an aggregate leak-off coefficient C_A of the fracture-reservoir interface, which is expected to be a function of reservoir characteristics and characteristics of the interface. The new form of the equation is

$$L(t) = \frac{q_i t^{0.5}}{2\pi C_A} \qquad (12)$$

which suggests that the **fracture growth speed is largely independent of most caprock characteristics**, including mechanical properties (e.g. stiffness) and features determining the total fracture height. As discussed in the previous section, an open hydraulic fracture's transmissivity is tremendously high compared with the overall transmissivity of the reservoir. The effect of a reduction of fracture height on fracture transmissivity can be easily compensated by a minimal increase of the net pressure (e.g. 10's of kPa). This would only have a very small effect on the reservoir overpressure (reservoir overpressure being approximately 10 MPa at the fracture-reservoir interface for the baseline simulation), so the interaction between the fracture and the reservoir is only minimally affected by the fracture height. Note that S_{hmin} in the caprock does affect the fracture growth rate through its effects on the leak-off coefficient: a greater difference between S_{hmin} and P_{ri} causes faster leak-off.

The evolution of the length in the baseline simulation is shown in Figure 7 (denoted by black crosses), where the length is computed as the fracture area divided by the fracture height. Equation (12) fits the baseline simulation results very well with C_A=0.046 $m^2/s^{0.5}$, especially when the fracture length is significantly greater than the height. The discrepancy between the simulation results and the analytical prediction in the early stage of the fracturing is likely caused by the PKN model's assumption of a rectangular fracture shape with a fixed height. In the early stage of the injection, the hydraulic fracture is radial in shape (a half-penny-shaped fracture) so the equivalent length calculation and the direct length comparison are not strictly appropriate.

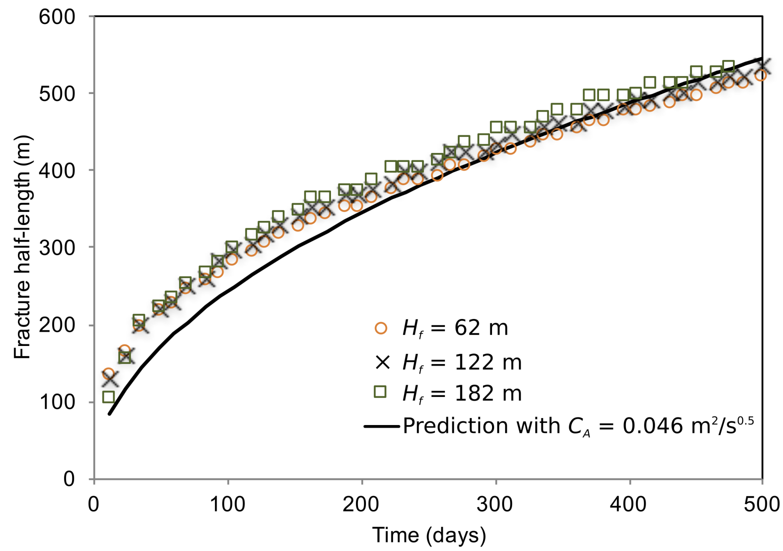

Figure 7 The propagation rate of the hydraulic fracture for various fracturable heights in the caprock. Fitting equation (12) to the baseline (H_f = 122 m) simulation results yields the solid line. The fracture height H_f is the summation of the caprock fracturable height (60, 120, and 240 m) and the thickness of the fracture-reservoir interface (2 m).

To enable quantitative interpretation of the C_A coefficient, we consider the following comparison with the Carter's leak-off coefficient C_L. C_L is usually determined experimentally in the field or in a laboratory environment. Under the assumption of one-dimensional diffusion, it can be analytically deduced as

$$C_{Lr} = \Delta P \left(\frac{k_r \phi_r c_t}{\pi \mu_r}\right)^{0.5} \qquad (13)$$

where ΔP is the difference between the fluid pressure acting on the fracture wall and the original reservoir pressure which is assumed to be constant; k_r is the permeability of the reservoir; ϕ_r is the reservoir porosity; c_t is the total (fluid and pore) compressibility; and μ_r is the dynamic viscosity of the fluid. Plugging in the relevant parameters associated with the numerical models, namely ΔP=10 MPa, k_r = 15 mD, n_r = 0.15, $c_t = 1.25\times10^{-8}$ Pa^{-1} and μ_r = 0.5 cP, we obtain C_{Lr} = 1.34 mm/s$^{0.5}$. Integrating the leak-off coefficient over the thickness (24 m) of the reservoir, we get $C_{Lr}H_r$ = 0.032 m^2/s$^{0.5}$, which is 30% smaller than the C_A value fitted to the simulation results. This discrepancy reflects the fact that the fluid diffusion into the reservoir is not one-dimensional as assumed in equation (13). The pore pressure plumes in both Figure 5 and Figure 8 show clear 2D diffusion patterns, so the 1D diffusion assumption has yielded an underestimate of the actual leak-off coefficient. Similar phenomena have been reported in Carrier and Granet [2012]. Another discrepancy between the modeling scenario and the 1D leak-off formula is that the interface area is only a small fraction of the reservoir thickness. This factor would result in a smaller leak-off coefficient than the predicted value, but the results indicate that it is not a very significant factor. Nevertheless, equation (13) provides a useful approximation of the leak-off coefficient to be used in equation (12).

To test the hypothesis that the fracture growth rate is independent of fracture height, we run two additional simulations with the fracturing barrier 60 m (model IV) and 180 m (model V) above the reservoir (H_f= 62 m and 182 m), respectively and otherwise identical parameters to those of the baseline case. The growth rate of the hydraulic fractures for these two scenarios is also plotted in Figure 7. The results show that the fracture growth rate is indeed insensitive to the fracture height. The fracture aperture distribution and reservoir pore pressure distribution for two different fracture heights after 208 days are shown in Figure 8. As expected, a reduction in fracture height reduces the aperture compliance proportionally, which results in a moderate increase in net pressure to drive the same flow rate through smaller aperture. The reservoir pressure distribution, however, remains largely unchanged with the variation of the fracture height. Therefore, equation (12) proves to adequately predict the caprock hydraulic fracture propagation rate based on reservoir characteristics and pumping parameters, at least for the idealized scenarios that we have analyzed so far.

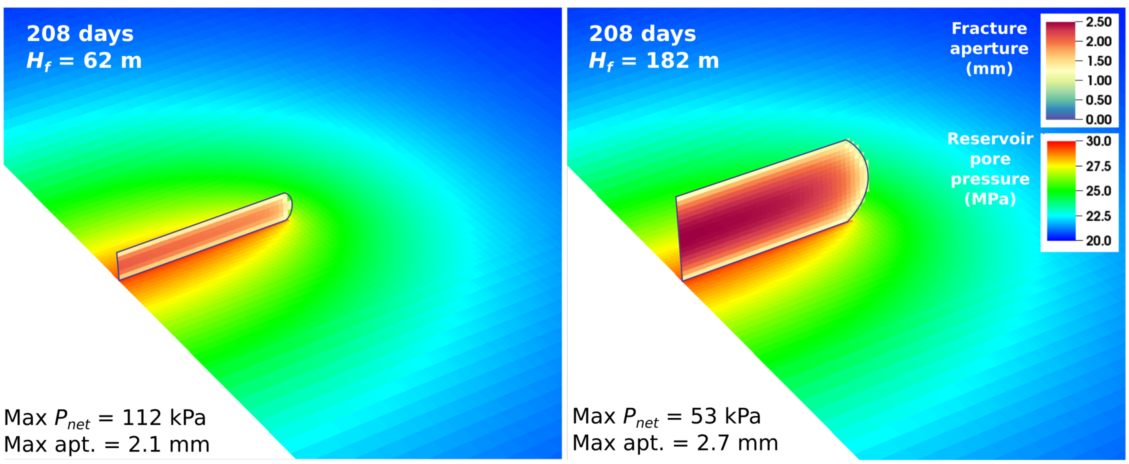

Figure 8 Fracture aperture distribution and reservoir pore pressure distribution for two different fracture heights (62 m and 242 m, corresponding to fracturing barrier at 60 m and 240 m above the reservoir, respectively), 208 days into injection. Pore pressure is shown on a slice near the top of the reservoir. For each case, the maximum fracture net pressure and the maximum aperture across the fracture are annotated.

7 The effects of spatial variation of S_{hmin}

All the previous discussions assumed the vertical gradient of S_{hmin} to be the same as the hydrostatic gradient of the fluid and no horizontal variation of S_{hmin}. This section explores how the spatial distribution of S_{hmin} affects the growth of the caprock hydraulic fracture and the interactions between the fracture and the reservoir.

7.1 Vertical variation of S_{hmin}

We first consider the scenario in which S_{hmin} impedes the upward growth of the hydraulic fracture, namely when $-dS_{hmin}/dz < \rho_f g$ where g is the gravitational acceleration. Note that the sign convention dictates that $dS_{hmin}/dz < 0$ means S_{hmin} increases with depth as the z-axis points upwards. Under this condition ($-dS_{hmin}/dz < \rho_f g$), an increase of fracture fluid pressure (compared with the baseline) would have two consequences. First, it allows S_{hmin} to be exceeded at a higher location and thereby a greater fracture height. Second, for a given fracture height, a higher net pressure generates a larger aperture. Both effects reduce the flow impedance of the fracture. Therefore, under a given S_{hmin} gradient and injection rate, the fluid pressure will assume a value that generates sufficient fracture height, aperture, and pressure gradient along the fracture to accommodate the injection rate. The equilibrium state under a greater dS_{hmin}/dz value (less negative or more positive) entails smaller fracture height and larger aperture. In Figure 9 the brown curve qualitatively depicts, under a constant injection rate, the fracture net pressure as a function of the fracture height. The shape of this curve is affected by stiffness of the rock, rheology of the fluid (CO_2), injection rate, among other factors. The blue curves show two hypothetical profiles of S_{hmin} (after the hydrostatic gradient corresponding to the density of supercritical CO_2 has been subtracted) in the caprock. The expected hydraulic fracture height in the caprock is approximately at where the brown curve and the blue curve first intersect.

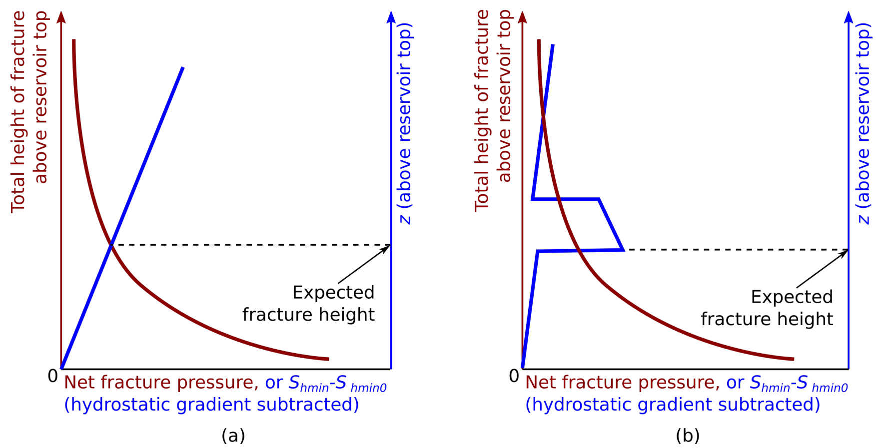

Figure 9 Two hypothetical cases to illustrate how the vertical distribution of S_{hmin} in the caprock determines the height of the hydraulic fracture: (a) if S_{hmin} smoothly changes with depth, and (b) if S_{hmin} suddenly changes at rock formation interfaces to form a stress barrier. S_{hmin0} is S_{hmin} at the bottom of the caprock.

If the stress gradient is such that $-dS_{hmin}/dz > \rho_f g$, it drives the hydraulic fracture to grow upwards. Because it takes less pressure (or more strictly speaking, less hydraulic head) to fracture the rock at a higher location, the caprock fracture tends to continue the upward propagation instead of fracturing the rock immediately above the reservoir. However, as the storage capacity of a fracture is small, the fracture growth that does not increase fracture-reservoir interface is much faster than that connected to the reservoir. The growth will soon be halted when it encounters a fracture barrier or a significant storage volume in the form of a porous and permeable formation. When encountering a fracture barrier, the fracture continues to dilate with increasing net pressure until the pressure is high enough to fracture the caprock immediately above the reservoir so that the injected fluid can flow back to the reservoir and release the excess pressure. The scenario of encountering a storage volume is essentially transporting the injected fluid to a shallower reservoir through the fracture.

7.2. Randomly distributed S_{hmin} in the caprock

When S_{hmin} is randomly distributed both vertically and horizontally, the system behavior becomes more complex but the principles governing the processes remain unchanged. To illustrate the fracturing and flow processes under such conditions, we impose a random perturbation to the caprock S_{hmin} field based on the baseline simulation in section 5 so that 1) the mean S_{hmin} in the caprock is unchanged, 2) the standard deviation of S_{hmin} is 0.5 MPa, 3) the auto-correlation lengths of S_{hmin} are 60 m and 120 m in the vertical and horizontal directions, respectively, and 4) the fracture barrier is still at 120 m above the reservoir. The generation of such auto-correlated random fields has been described in Guo et al. [2016] and is not repeated here. The distribution of resultant *in situ* S_{hmin} in the caprock is shown in Figure 10(a). Similar to the treatments for the baseline scenario in section 5, we remove the gravitational terms from the flow solutions, which dictates that the actual S_{hmin} profile being modeled has a vertical gradient identical to the hydrostatic pressure gradient corresponding to the surrogate fluid density. In other words, the mean S_{hmin} gradient and the fracture flow hydrostatic gradient cancel out and do not play an explicit role in the simulation.

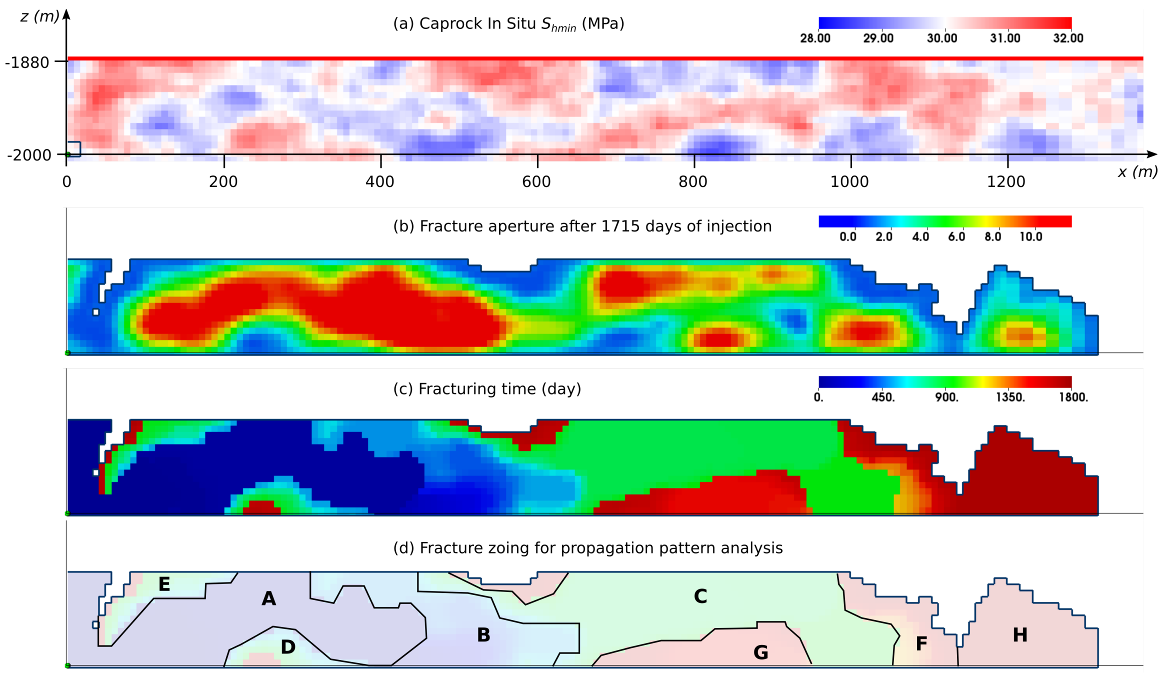

Figure 10 Simulation results for randomly distributed S_{hmin}. Quantities associated with the fracture are projected onto the x-z plane. (a) *In situ* minimum principle stress S_{hmin} in the fracturable portion of the caprock; (b) the distribution of fracture aperture after 1715 days of injection, i.e. in the end of the simulation; (c) the distribution of fracturing time along the caprock hydraulic fracture; and (d) zoning of the hydraulic fracture area based on fracturing time.

As expected, the growth of the caprock fracture and its interaction with the reservoir are not as smooth and steady as in the baseline simulation. Figure 10(b) shows the distribution of fracture aperture after 1715 days (end of simulation) of pumping. Coordinating the patterns in Figure 10(a) and Figure 10(b) reveals that large aperture tends to develop at locations with originally relatively low S_{hmin}. “Pockets” of large apertures are separated by high-stress zones, with the latter acting as bottlenecks for flow. The largest aperture at that time is 14 mm, several times greater than that of the baseline case which employed the same mean stress and injection rate. This is because the fracture fluid pressure is controlled by the need to fracture high-stress zones. As pressure loss across the fracture is small, the net pressure (which dilates the fracture aperture) can be as high as several MPa's at low stress zones, resulting in large local aperture. Figure 10(c) shows the time of fracturing across the final fracture geometry, and in Figure 10(d) we identify eight zones based on distinct growth patterns. For instance, the fracture area in zone A and that in zone C are characterized by uniform colors in Figure 10(c), indicating each is created over a short period of time (i.e. fast growth). On the other hand, the relatively smooth color gradients in zone B and zone F suggest gradual fracture growth.

Figure 11(a) shows the time history of injection pressure, where ten points are marked, denoting remarkable events during the injection that illustrate various interaction modes between caprock hydraulic fracture and reservoir under complex *in situ* stresses. Figure 11(b) shows separation of the fracture face elements as individual "events" (red dots) while the fracturing of the faces along the fracture-reservoir interface is highlighted as green squares. The shaded area in Figure 11(b) illustrates the evolution of the horizontal extent of the fracture-reservoir interface, whose correspondences with the interface fracture events is evident in the figure. Note that the "fracturing events" discussed here are mere discretized fracturing steps in the numerical model; investigating the relationship between these events and actual "seismic" or "microseismic" events associated with underground fluid injection is beyond the scope of the current work.

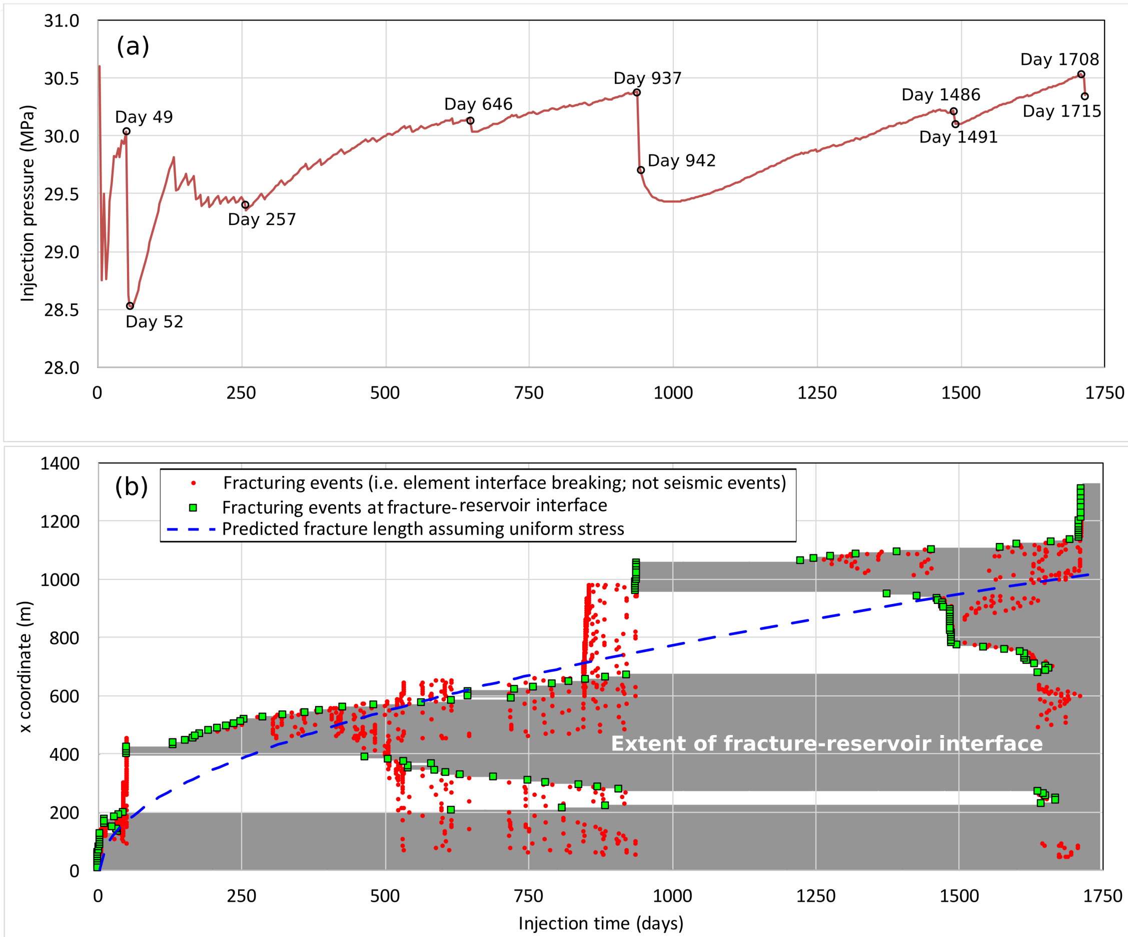

Figure 11 Selected time histories of the simulation with randomly distributed S_{hmin}. (a) The evolution of bottomhole injection pressure with selected times denoted corresponding to the snapshots in Figure 12. (b) The distribution of fracturing events (red dots) in terms of x-coordinate and fracturing time. Note that the fracturing events in this context refers to occurrences of fracture growth and the associated mesh topology change, and do not imply seismic events. Fracturing events at the fracture-reservoir interface are highlights as green squares. The shaded area denotes the evolution of the horizontal extent of the fracture-reservoir interface. The predicted fracture length evolution based on equation (12) calibrated by the baseline simulation is shown as the blue dashed line.

The following analysis is best illustrated by a combined review of Figure 11 and Figure 12. The first highlighted stage of the fracture propagation took place between day 49 of the injection and day 52. On day 49, the top of the fracture has reached x=320 m while the bottom (interface with reservoir) was still bounded by a stress barrier at x = 200 m. The accumulation of pressure allowed the fracture to propagate through the upper portion to interface with the reservoir again at x = 420 m. The availability of unpressured reservoir volume resulted in an instantaneous pressure drop at day 52 and gradual pressure increase thereafter as newly accessible reservoir volume was pressurized. From day 52 to day 257, the fracture slowly propagated within a low-stress region at the bottom of the zone B, during which the pressure remained relative low and aperture small. From day 257 to day 646, the fracture-reservoir interface grew very slowly (evident in Figure 11(b)), limited by a high-stress barrier at x = 550 m, with the injection pressure continuing to increase. After day 646, pressure was high enough to allow the fracture to grow backwards (negative x direction) to cover zone D. Although on day 937 the upper portion of the fracture had grown to x = 980 m, the fracture-reservoir interface only reached x = 650 m. On day 942 as shown in Figure 12, the accumulated pressure allowed the fracture to break the high-stress barrier at x = 980 m and the fracture established new interface with the reservoir up to x = 1080 m. As another barrier exists ahead of the fracture front, similar processes repeated thereafter.

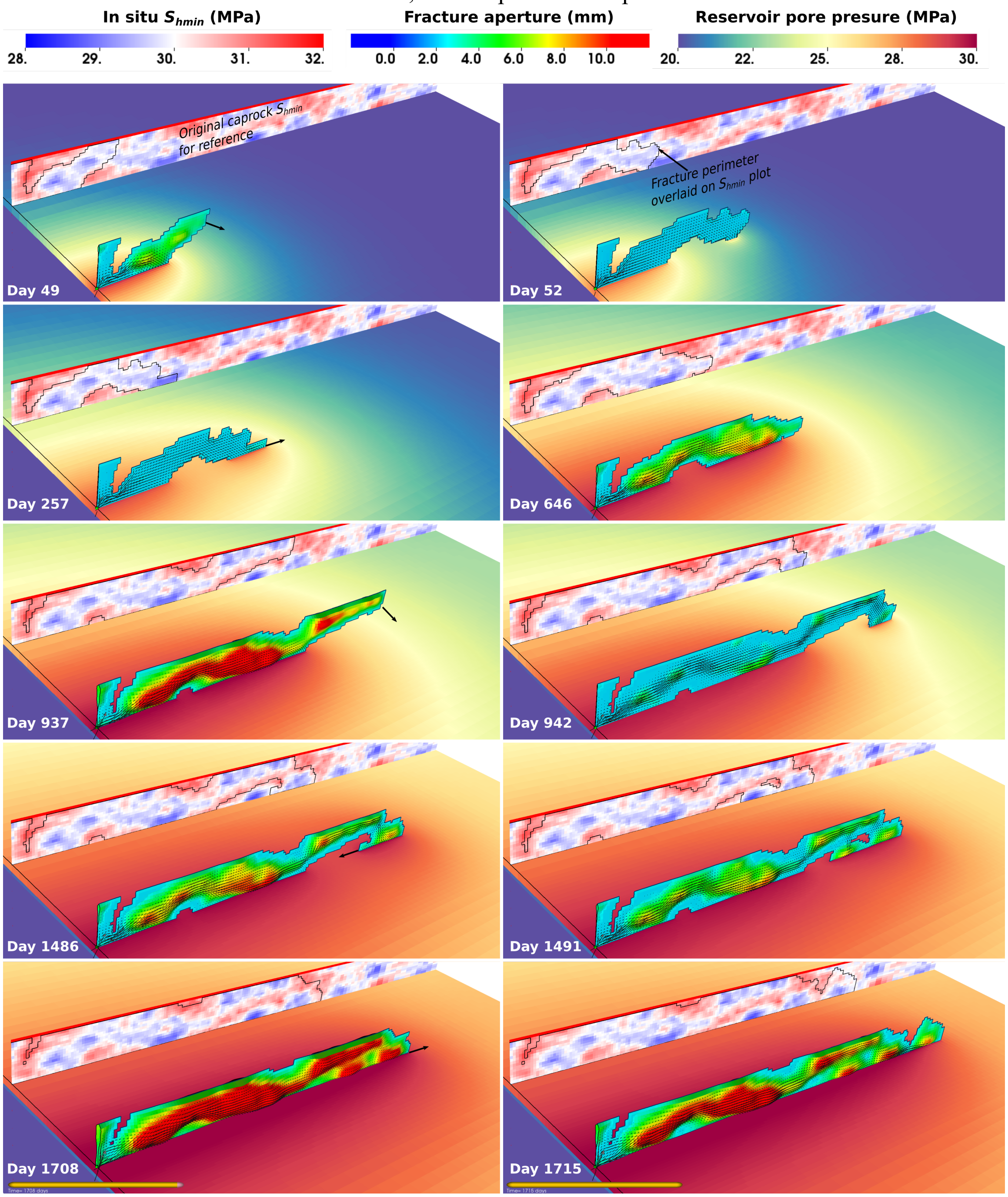

Figure 12 Snapshots of the caprock fracture extent, fracture aperture, and reservoir pore pressure on ten days are also denoted in Figure 11(a). The large black arrows in selected sub-figures indicate the most

significant subsequent fracture growth directions. The original *in situ* S_{hmin} is shown in a "slice" plane placed 400 m from the hydraulic fracture plane, on which the perimeter of the fracture is overlaid. The fracture is colored based on the aperture and the deformation is magnified by 4,000 times. On the fracture plane are vectors representing the flow direction and flow rate.

The caprock fracture growth under heterogeneous *in situ* stress appears to be much more complicated than that under more idealized conditions as presented in previous sections. However, the same principles governing the interaction between the fracture and the reservoir apply. When fracture growth is limited by stress barriers, fluid flowing into the reservoir through an interface of a fixed length results in continuous pressure increase, until the pressure is sufficiently high to allow the fracture to break into/across high-stress regions and eventually create new fracture-reservoir interface lengths. The creation of fracture into reservoir causes the injection pressure to decrease temporarily but that portion of the reservoir eventually saturates and motivates another episode of fracture growth. As shown in Figure 11(a), although the injection pressure fluctuates remarkably between temporary fracture containment by stress barriers and fast breakthroughs, the range of variation is generally within the mean S_{hmin} value ± standard deviation of S_{hmin}, echoing with the earlier observation that caprock S_{hmin} dictates injection pressure. Additionally, equation (12) with parameters calibrated based on the baseline simulation with homogeneous S_{hmin} provides a reasonable estimate of the fracture length development as shown Figure 11(b).

8 Concluding remarks

8.1 Summary of technical findings

In this work, we studied the enabling conditions, processes, and mechanisms of hydraulic fracturing during CO_2 injection into a saline reservoir with relatively low permeability. The study utilizes fully-coupled numerical simulation of hydraulic fracturing and reservoir flow with a single-phase surrogate fluid.

First, we calculated the near-well pressure evolution for fluid injection into a moderately low-permeability saline reservoir. We found that under certain conditions common to commercial carbon storage applications, the near-well pressure could be higher than the fracturing pressure of the reservoir and/or the caprock. When the *in situ* minimum horizontal principal stress S_{hmin} in the reservoir formation is significantly lower than that in the caprock, it is possible to create a hydraulic fracture within the reservoir rock without fracturing the caprock. Such a fracture could be sufficient to provide efficient and effective access to the reservoir. However, a poroelastic analysis suggests that sustaining an open fracture in the reservoir will require continuously increasing pressure that may eventually be high enough to fracture the caprock.

Once initiated, the caprock hydraulic fracture exhibits pressure-limiting behavior dictating that the fracture fluid pressure remains only slightly higher than the pressure required to maintain an open fracture and is insensitive to any practical variation of the injection rate. However, because other energy dissipation mechanisms, including wellbore friction loss, entry loss, and the porous medium flow regime between wellbore exits and fracture entrances, are dependent on the flow rate, the wellhead injection pressure could still be sensitive to the injection rate. The propagation behavior of a caprock hydraulic fracture connected to a CO_2 storage reservoir is analogous to that of the PKN hydraulic fracture in the leak-off-dominated regime. The fracture extends at such a rate that the creation of new flow interface between the fracture and the reservoir accommodates the injection rate. In essence, a hydraulic fracture provides an economical (i.e. very low energy dissipation across the fracture) and effective means for the injected fluid to access reservoir storage that is far from the injection point. Under a constant injection rate, the fracture length is proportional to the square root of elapsed time, proportional to the injection rate, and inversely proportional to an aggregate leak-off coefficient that represents the reservoir's ability to accommodate additional fluid at the given overpressure and hydraulic impedance at the fracture-reservoir interface. The aggregate leak-off coefficient for the fracture-reservoir interface can be approximated with the Carter's leak-off coefficient of the reservoir multiplied by the reservoir thickness. The most important implication of this finding is that the hydraulic fracture propagation rate is nearly independent of the fracture height and mechanical properties of the caprock.

Heterogeneity in caprock's *in situ* stress field induces fluctuations in the growth rate and injection pressure. The fracture can be temporarily contained by high-stress barriers while this leads to increasing pressure until it is sufficient to break the barriers. When the stress barrier is overcome, the potential energy accumulated in the fracture fluids drives rapid fracture growth until the fracture connects to unpressurized reservoir volume. Subsequently, the fracture fluid pressure decreases and the fracture is temporarily contained again, starting another episode of the containment-fast growth cycle. However, the overall behavior of such heterogeneous caprock fracture remains consistent with that under idealized uniform stresses, except that fracture aperture in low-stress "pockets" can be significantly larger than that in a smooth stress field. Although not investigated in the current work, the compartmentalization of reservoirs [Castelletto et al., 2013] could also cause fluctuations in fracture growth rate.

To quantitatively express the findings in a concise fashion, we define the following quantities:

- P_{ri}, initial reservoir pore pressure;
- P_{frac}, fluid pressure requires to initiate and sustain a hydraulic fracture;
- S_{hmin_r}, minimum principle stress in the CO_2 storage reservoir;
- S_{hmin_c}, minimum principle stress in the caprock immediately above the reservoir.

The following relationships generally hold:

1) If the reservoir rock is fracturable, $P_{frac} > S_{hmin\_r}$, and the difference tends to increase over time due to poroelasticity.
2) If a hydraulic fracture cannot be sustained in the reservoir rock with a pressure $P_{frac} < S_{hmin\_c}$, then caprock fracturing takes place and $P_{frac} \approx S_{hmin\_c}$.
3) Because typically $P_{frac} - S_{hmin\_c} << S_{hmin\_c} - P_{ri}$, $S_{hmin\_c} - P_{ri}$ ($\approx P_{frac} - P_{ri}$) determines both the reservoir storage capacity and the hydraulic fracture propagation rate.

8.2 Relevance to CO2 storage design and site characterization

The findings of this work could have important implications for the design of geological carbon storage projects. Because flow along an open hydraulic fracture is tremendously more efficient than flow within a porous medium in delivering fluid to far-field reservoir, injection through hydraulic fracturing could improve the CO_2 injection and storage capacity. The insensitivity of the injection pressure to the fracture height means that vertical containment of the fracture has no negative impact on the economics. In retrospect, this suggests that the arbitrary choice of fracture barrier location in the models did not significantly affect the results. Nevertheless, the identification and evaluation of fracture barriers in the caprock would be a critical issue in GCS project design, and deserve systematic studies.

The most desirable scenario is that a hydraulic fracture can be sustained exclusively within the reservoir rock (i.e. no caprock fracturing) at an injection pressure lower than S_{hmin_c} (minimum principal stress in caprock). Therefore, studying the fracturability of the reservoir rock, both as a generic scientific subject and for specific rock formations at the project level, is of a remarkable importance. If sustaining a hydraulic fracture exclusively within the reservoir under $P_{frac} < S_{hmin\_c}$ has proven to be impossible for a site, the focus of the site characterization would be to investigate whether certain features of the caprock formation, such as stress gradient or persistent stress barriers, can effectively bound the vertical growth of the hydraulic fracture(s) without causing significant CO_2 leakage. Nevertheless, the current work only intends to reveal the mechanisms governing the propagation of caprock fracture and its interaction with storage reservoir. Whether geologic carbon storage through geomechanically contained caprock fracturing is a safe, viable engineering approach requires more systematic, rigorous studies.

Acknowledgments:

This study was originally motivated by extensive discussion with Dr. Joshua A. White of LLNL, and we would like to acknowledge his helpful input. Dr. Susan A. Carroll of LLNL also provided important guidance to this work. This work was partly supported by LLNL LDRD project "*High-Fidelity Fracture Model for Hydraulically Fractured Shale Reservoirs*" (16-ERD-014). This manuscript has been authored by Lawrence Livermore National Security, LLC under Contract No. DE-AC52-07NA2 734-I with the US. Department of Energy. The United States Government retains, and the publisher, by accepting the article for publication, acknowledges that the United States Government retains a non-exclusive, paid-up, irrevocable, world-wide license to publish or reproduce the published form of this manuscript, or allow others to do so, for United States Government purposes This work is LLNL report LLNL-JRNL-738072.

References:

Boait, F. C., N. J. White, M. J. Bickle, R. A. Chadwick, J. A. Neufeld, and H. E. Huppert (2012), Spatial and temporal evolution of injected CO_2 at the Sleipner Field, North Sea, J. Geophys. Res., 117, B03309, doi:10.1029/2011JB008603.

Biot, M.A. (1941). "General Theory of Three-Dimensional Consolidation". Journal of Applied Physics. 12 (2): 155–164. doi:10.1063/1.1712886.

Bryant, S. L., Lakshminarasimhan, S., and Pope, G. A. (2008). Buoyancy-Dominated Multiphase Flow and Its Effect on Geological Sequestration of CO2, SPE Journal, 13(4), 447–454, doi:10.2118/99938-PA.

Carter, R.D.: "Derivation of the General Equation for Estimating the Extent of the Fractured Area," Appendix I of "Optimum Fluid Characteristics for Fracture Extension," Drilling and Production

Practice, G.C. Howard and C.R. Fast, New York, New York, USA, American Petroleum Institute (1957), 261–269.

Carrier, B., & Granet, S. (2012). Numerical modeling of hydraulic fracture problem in permeable medium using cohesive zone model. Engineering Fracture Mechanics, 79, 312–328. http://doi.org/10.1016/j.engfracmech.2011.11.012

Castelletto N., G. Gambolati, and P. Teatini (2013), Geological CO_2 sequestration in multi-compartment reservoirs: Geomechanical challenges, J. Geophys. Res. Solid Earth, 118, 2417–2428, doi:10.1002/jgrb.50180.

Celia, M. A., Bachu, S., Nordbotten, J. M., & Bandilla, K. W. (2015). Status of CO 2 storage in deep saline aquifers with emphasis on modeling approaches and practical simulations. Water Resources Research, 51(9), 6846–6892. http://doi.org/10.1002/2015WR017609

Chiaramonte, L., White, J. A. and Trainor-Guitton, W. (2015), Probabilistic geomechanical analysis of compartmentalization at the Snøhvit CO_2 sequestration project. J. Geophys. Res. Solid Earth, 120: 1195–1209. doi: 10.1002/2014JB011376.

Detournay, E. (2004). Propagation Regimes of Fluid-Driven Fractures in Impermeable Rocks. International Journal of Geomechanics, 4(1), 35. http://doi.org/10.1061/(ASCE)1532-3641(2004)4:1(35)

Detournay, E., & Cheng, A. H. D. (1991). Plane strain analysis of a stationary hydraulic fracture in a poroelastic medium. *International Journal of Solids and Structures*, *27*(13), 1645–1662. http://doi.org/10.1016/0020-7683(91)90067-P

Durucan, S., Shi, J. Q., Sinayuc, C., & Korre, A. (2011). In Salah CO_2 storage JIP: Carbon dioxide plume extension around KB-502 well - New insights into reservoir behaviour at the In Salah storage site. Energy Procedia, 4, 3379–3385. http://doi.org/10.1016/j.egypro.2011.02.260

Ehlig-Economides, C., & Economides, M. J. (2010). Sequestering carbon dioxide in a closed underground volume. Journal of Petroleum Science and Engineering, 70(1–2), 123–130. http://doi.org/10.1016/j.petrol.2009.11.002

Eiken, O., Ringrose, P., Hermanrud, C., Nazarian, B., Torp, T. A., & L. Høier (2011). Lessons Learned from 14 years of CCS Operations: Sleipner, In Salah and Sn??hvit. Energy Procedia, 4, 5541–5548. http://doi.org/10.1016/j.egypro.2011.02.541

Fisher, M. K., & Warpinski, N. R. (2012). Hydraulic-Fracture-Height Growth: Real Data, *SPE Prod. Oper*., 27(01), 8–19, doi:10.2118/145949-PA.

Fu, P., Johnson, S. M., & Carrigan, C. R. (2013). An explicitly coupled hydro-geomechanical model for simulating hydraulic fracturing in arbitrary discrete fracture networks. International Journal for Numerical and Analytical Methods in Geomechanics, 37(14), 2278–2300. http://doi.org/10.1002/nag.2135

Guo, B., Fu, P., Hao, Y., Peters, C. A., & Carrigan, C. R. (2016). Thermal drawdown-induced flow channeling in a single fracture in EGS. *Geothermics*, *61*, 46–62. http://doi.org/10.1016/j.geothermics.2016.01.004

Han, W. S., G. A. Stillman, M. Lu, C. Lu, B. J. McPherson, and E. Park (2010), Evaluation of potential nonisothermal processes and heat transport during CO_2 sequestration, J. Geophys. Res., 115, B07209, doi:10.1029/2009JB006745.

Haszeldine, R. S. (2009). Carbon Capture and Storage: How Green Can Black Be? Science, 325(5948), 1647–1652. http://doi.org/10.1126/science.1172246

Hubbert, K. M., & Willis, D. G. (1957). Mechanics of Hydraulic Fracturing. Transactions Of The American Institute Of Mining And Metallurgical Engineers, 210(6), 153–163.

Iding, M., & Ringrose, P. (2010). Evaluating the impact of fractures on the performance of the In Salah CO_2 storage site. International Journal of Greenhouse Gas Control, 4(2), 242–248. http://doi.org/10.1016/j.ijggc.2009.10.016

International Energy Agency, 2010. Energy Technology Perspectives 2010: Scenarios and Strategies to 2050. International Energy Agency, Paris, France.

Krueger, R. 2004. Virtual crack closure technique: History, approach, and applications. *Appl. Mech. Rev.*, *57*(2), 109, doi:10.1115/1.1595677.

Lecampion, B., J. Desroches, R. G. Jeffrey, and A. P. Bunger (2017), Experiments versus theory for the initiation and propagation of radial hydraulic fractures in low-permeability materials, J. Geophys. Res. Solid Earth, 122, 1239–1263 doi:10.1002/2016JB013183.

McGrail, B. P., H. T. Schaef, A. M. Ho, Y.-J. Chien, J. J. Dooley, and C. L. Davidson (2006), Potential for carbon dioxide sequestration in flood basalts, J. Geophys. Res., 111, B12201, doi:10.1029/2005JB004169.

Morris, J. P., Hao, Y., Foxall, W., & McNab, W. (2011). A study of injection-induced mechanical deformation at the In Salah CO_2 storage project. International Journal of Greenhouse Gas Control, 5(2), 270–280. http://doi.org/10.1016/j.ijggc.2010.10.004

Nordgren, R. P. (1972). Propagation of a Vertical Hydraulic Fracture. Society of Petroleum Engineers Journal, 12(4), 306–314. http://doi.org/10.2118/3009-PA

Okwen, R. T., Stewart, M. T., and Cunningham, J. A. (2011). Temporal variations in nearwellbore pressures during CO_2 injection in saline aquifers, Int. J. Greenh. Gas Control, 5(5), 1140–1148, doi:10.1016/j.ijggc.2011.07.011.

Orr, F. M. (2009). Onshore Geologic Storage of CO_2. Science, 325(5948), 1656–1658. http://doi.org/DOI 10.1126/science.1175677

Pacala, S., & Socolow, R. (2004). Stabilization Wedges: Solving the Climate Problem for the Next 50 Years with Current Technologies. Science, 305(5686), 968–972. http://doi.org/10.1126/science.1100103

Pan, P.-Z., Rutqvist, J., Feng, X.-T., & Yan, F. (2013). Modeling of caprock discontinuous fracturing during CO_2 injection into a deep brine aquifer. International Journal of Greenhouse Gas Control, 19, 559–575. http://doi.org/10.1016/j.ijggc.2013.10.016

Perkins, T.K., & Kern, L.R. (1961). Widths of Hydraulic Fractures. Journal of Petroleum Technology, 13(9), 937–949. http://doi.org/10.2118/89-PA

Renshaw, C. E., and C. F. Harvey (1994), Propagation velocity of a natural hydraulic fracture in a poroelastic medium, J. Geophys. Res., 99(B11), 21667–21677, doi:10.1029/94JB01255.

Rinaldi, A. P., & Rutqvist, J. (2013). Modeling of deep fracture zone opening and transient ground surface uplift at KB-502 CO_2 injection well, In Salah, Algeria. International Journal of Greenhouse Gas Control, 12, 155–167. http://doi.org/10.1016/j.ijggc.2012.10.017

Ringrose, P. S., Mathieson, A. S., Wright, I. W., Selama, F., Hansen, O., Bissell, R., Saoula, N., & J. Midgley. (2013). The in salah CO_2 storage project: Lessons learned and knowledge transfer. Energy Procedia, 37, 6226–6236. http://doi.org/10.1016/j.egypro.2013.06.551

Salimzadeh, S., Paluszny, A., & Zimmerman, R. W. (2017). Three-dimensional poroelastic effects during hydraulic fracturing in permeable rocks. International Journal of Solids and Structures, 108: 153-163. http://doi.org/10.1016/j.ijsolstr.2016.12.008

Settgast, R. R., Fu, P., Walsh, S. D., White, J. A., Annavarapu, C., & Ryerson, F. J. (2016). A fully coupled method for massively parallel simulation of hydraulically driven fractures in 3-dimensions. International Journal for Numerical and Analytical Methods in Geomechanics. http://doi.org/10.1002/nag.2557

Shi, J. Q., Sinayuc, C., Durucan, S., & Korre, A. (2012). Assessment of carbon dioxide plume behaviour within the storage reservoir and the lower caprock around the KB-502 injection well at In Salah. International Journal of Greenhouse Gas Control, 7, 115–126. http://doi.org/10.1016/j.ijggc.2012.01.002

Span, R., & Wagner, W. (1996). A New Equation of State for Carbon Dioxide Covering the Fluid Region from the Triple-Point Temperature to 1100 K at Pressures up to 800 MPa. *Journal of Physical and Chemical Reference Data*, *25*(6), 1509. http://doi.org/10.1063/1.555991

Verdon, J. P., Kendall, J.-M., Stork, A. L., Chadwick, R. A., White, D. J., & Bissell, R. C. (2013). Comparison of geomechanical deformation induced by megatonne-scale CO_2 storage at Sleipner, Weyburn, and In Salah. Proceedings of the National Academy of Sciences of the United States of America, 110(30), E2762-71. http://doi.org/10.1073/pnas.1302156110

Warpinski, N., Schmidt, R., & Northrop, D. (1982). In-Situ Stresses: The Predominant Influence on Hydraulic Fracture Containment, *J. Pet. Technol*., 34(3), doi:10.2118/8932-PA.

Warpinski, N. R., & Teufel, L.W. (1987). Influence of Geologic Discontinuities on Hydraulic Fracture Propagation, *J. Pet. Technol*., 39(2), 209–220, doi:10.2118/13224-PA.

Zimmerman, R.W. (2002) Fluid Flow in Porous Media, course notes for M.Sc. in Petroleum Enigineering. Department of Earth Science and Engineering, Imperial College, London.

Zhang, X., and R. G. Jeffrey (2012), Fluid-driven multiple fracture growth from a permeable bedding plane intersected by an ascending hydraulic fracture, J. Geophys. Res., 117, B12402, doi:10.1029/2012JB009609.

Zoback, M. D., & Gorelick, S. M. (2012). Earthquake triggering and large-scale geologic storage of carbon dioxide. Proceedings of the National Academy of Sciences of the United States of America, 109(26), 10164–8. http://doi.org/10.1073/pnas.1202473109

`